Journal of Scientific & Industrial Research
Vol. 78, October 2019, pp. 694-698

Thermal and Fluid Flow Analysis of Miller Teeth Shaped Ribbed Solar Air Heater- A CFD Approach

P J Bezbaruah*, R S Das and B K Sarkar

Department of Mechanical Engineering, National Institute of Technology Meghalaya
Shillong–793003, Meghalaya, India

Received 5 March 2018; revised 2 January 2019; accepted 14 June 2019

Present simulation work is based on qualitative as well as quantitative study on the thermohydraulic effect on a solar air heater due to a unique shape of repeated rib similar to the shape of Miller teeth over absorber plate. The overall efficiency is assessed by measuring thermohydraulic performance factor at different operating parameters which considers thermal as well as hydraulic performances. Numerical simulation is carried out using ANSYS FLUENT (ver. 18.1) varying the Reynolds number in the applicable range of 3800-18000, while relative pitch ratio (P/e) and relative roughness height (e/D) are within the range of 7.14-35.7 and 0.021-0.042 respectively. The effect of different roughness heights and roughness pitches of miller teeth shaped rib on the heat transfer and fluid flow characteristics of a solar air collector is analysed and detailed justification is presented using different contours derived.

Keywords: CFD, solar air heater, artificial roughness, thermohydraulic performance parameter

Introduction

Solar air collector is a device that contributes in harnessing the abundant and clean solar energy. Numerical investigations with different types of roughness have been carried out in the past [1-10] to enhance its performance. In the present study, effect of miller teeth shaped transverse ribs on thermohydraulic performance of a solar air collector is analysed using ANSYS FLUENT 18.1. Three different values of relative roughness height (e/D) and four different values of relative roughness pitch (P/e) are considered for the present investigation.

Computational Details

A 2-D computational domain as per ASHRAE standards [11] is modelled using ANSYS modeller and is shown in Figure. 1a. It is a rectangular domain and consist of three sections namely inlet, test and outlet section where the lengths are 225 mm, 280 mm and 115 mm respectively. Width of the domain is considered to be 20 mm and is constant throughout. The roughness elements are considered in the underside of absorber plate situated in the test section. The roughness elements are expected to enhance the turbulence inside the flow by blocking the fluid flow and prevent the formation of thermal boundary layer. Higher turbulence in the flow would result in heat transfer enhancement from absorber plate to the fluid domain. Remaining all other sides is considered to be smooth. The geometrical parameters of the ribs considered in the present investigation are: Rib height, e = 0.7 mm, 1 mm and 1.4 mm; Rib pitch, P = 10 mm, 15 mm, 20 mm and 25 mm; Relative roughness pitch, P/e = 7.14, 10, 10.71, 14.29, 15, 17.86, 20, 21.43, 25, 28.57 and 35.71; Relative roughness height, e/D = 0.021, 0.03 and 0.042. The basic governing equations of CFD namely continuity, momentum and energy equations as shown in Eq. (1), Eq. (2) and Eq. (3) respectively that are employed in the simulation process are solved using finite volume method.

$$\frac{\partial}{\partial x_i}(\rho u_i) = 0 \quad \ldots (1)$$

$$\frac{\partial}{\partial x_i}\left(\rho u_i u_j\right) = \frac{-\partial P}{\partial x_i} + \frac{\partial}{\partial x_j}\left[\mu\left(\frac{\partial u_i}{\partial x_j} + \frac{\partial u_j}{\partial x_i}\right)\right] + \frac{\partial}{\partial x_j}\left(-\rho u_i u_j\right) \quad \ldots (2)$$

$$\frac{\partial}{\partial x_i}\rho u_j T = \frac{\partial}{\partial x_j}\left[(\tau + \tau_t)\frac{\partial T}{\partial x_j}\right] \quad \ldots (3)$$

Following assumptions are considered in the present study:

a. Single phase, steady, incompressible and turbulent flow.

*Author for Correspondence
E-mail: bezbaruahparag@nitm.ac.in

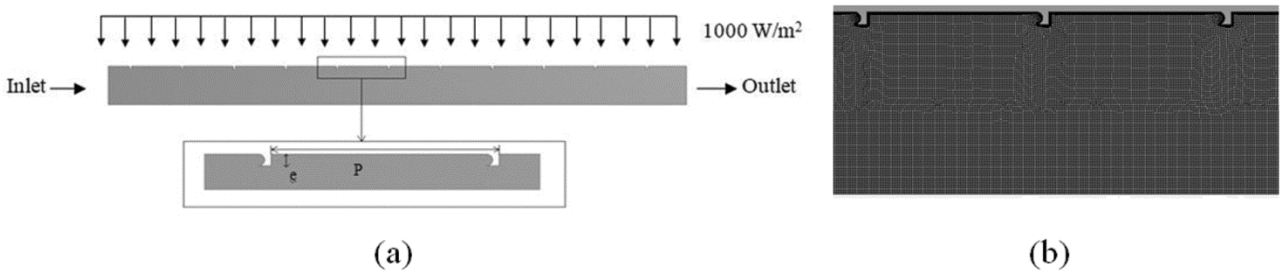

Fig. 1 — Computational domain (a) Schematic diagram (b) Non-uniform mesh structure.

b. Flow is thermally and hydraulically developed.
c. Properties of air and absorber plate are constant and do not vary along the flow.
d. Radiation from duct walls is negligible.

The boundary conditions that are applied in the present numerical simulation are as follows:

a. Air is selected as working fluid and enters the domain at 300 K and 1 atmospheric pressure.
b. No-slip condition is imposed on the duct walls.
c. Constant heat flux of 1000 W/m^2 [6-7] is imposed on absorber plate which is made of aluminium.
d. Adiabatic condition is implemented on all other duct walls.
e. Pressure outlet and velocity inlet (Re=3800, 5000, 8000, 12000, 15000 and 18000) are considered.

In the present investigation, velocity and pressure terms are coupled using SIMPLE algorithm. Discretization of convective terms of momentum and energy equations is done using second order upwind scheme whereas the diffusive terms are discretized using central difference scheme.

Grid Generation and Model Validation

In the present numerical study, non-uniform quadrilateral mesh is generated throughout the domain for thermal and flow computations. Non-uniform meshing is provided because of the complexity of the domain due to miller teeth shaped ribs. Quadrilateral mesh is preferred because of its ability to provide accurate results as compared to other mesh types. Inflation near the absorber plate is considered to capture the physics of laminar sub-layer as shown in Figure 1b. The inflation near the absorber plate is such provided that the y+ value is approximately 1. Grid independent test is done at three different sets of grid. The number of grids is varied from 142,565 to 398,363. It is found that with increase in number of grids from 322,544, the variations in results are less than 1%. For further simulation, 322,544 number of grids is considered. Figure. 1b shows the mesh structure used in the present simulation. The simulated values of Nusselt number, Nu and friction factor, f for flat plate duct using *k-ε* RNG turbulence model with enhanced wall treatment are found to be in good agreement with that of empirical formulas (Dittus-Boelter correlation [3] and Modified Blasius correlation [4]) and experimental results of Gawande *et al*. [3] as shown in Figure. 2. The *k-ε* RNG turbulence model with enhanced wall treatment is also suggested in other literatures [4-7]. So *k-ε* RNG turbulence model with enhanced wall treatment is employed for further investigation.

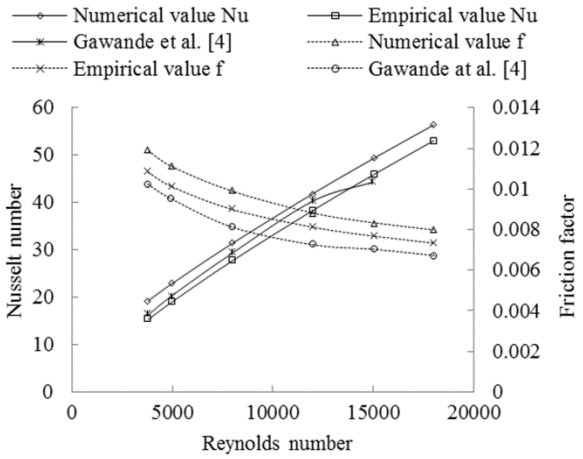

Fig. 2 — Validation of numerical results for flat plate solar air heater.

Results and Discussion

A quantitative as well as qualitative study on the change in thermal and fluid flow characteristics due to the presence of miller teeth shaped transverse ribs in solar air collector using CFD code is done. The effect of operating parameter like Reynolds number and geometrical parameters like P/e and e/D on the heat transfer coefficient, frictional resistance and overall performance is discussed.

Variation in Thermal and Hydraulic Performance

Nusselt number, Nu is the ratio of convective heat transfer to conductive heat transfer across a surface. It

gives the measure of heat transfer across a boundary. Whereas friction factor, f helps in predicting the frictional energy loss in a duct. In the present investigation deviation of heat transfer coefficient is shown in the form of Nu and that of flow friction characteristics is depicted using f. Table 1 shows the variation in Nu with respect to P/e at different Re. It is observed that with increase in Re, Nu increases for every value of e/D and P/e. Increase in Re increases the turbulence inside the flow domain resulting in increase in Nu. Turbulence inside the flow breaks restricts the formation of laminar sub-layer. With increase in Re, turbulent energy and turbulent dissipation rate increases resulting in increase in turbulent intensity. Same observation is made for each geometrical consideration in the present investigation. A maximum Nu value of 92.82 is observed for e/D=0.021 and P/e=14.29 at Re=18000. Whereas for e/D=0.03 and 0.042, maximum Nu is observed at P/e=10 and P/e=7.14 at Re=18000. It can be seen in Table 1 (a,d,g,j), that with increase in P/e for e/D=0.021, Nu decreases for a particular value of Re. However, higher roughness height shows a different trend for lower Re. With increase in P/e, Nu increases and then starts decreasing due to decrease in number of reattachment points. For Re=3800, the maximum Nu of 30.72 is achieved at e/D=0.042 and P/e=14.29. When compared to smooth duct, a percentage increase of 64.5% is noted due to the presence of miller teeth shaped ribs with P/e=14.29 and e/D=0.021 at Re=18000 whereas an increase in 59.6% is observed at Re=3800 for e/D=0.042 and P/e=14.29. From the values of Nu, it is clear that there is a significant enhancement due to the presence of ribs. With increase in Re, turbulent intensity increases. Moreover, due to the presence of roughness there is a local enhancement of turbulent intensity in the downstream of each roughness due to vortex formation. Figure. 3 shows the contours of velocity at different P/e for a particular value of e/D=0.021 and Re=12000. It can be observed that due to the presence of miller teeth shaped roughness there is a formation of longitudinal vortex in the vicinity of every roughness. It leads to increase the turbulent intensity in the back stream of every roughness element. The vortices break the laminar sub-layer resulting in higher heat transfer in that area. Table 1 also shows the variation of friction factor with P/e at different values of Re. It is found that, for same value of P/e, e/D=0.021 gives the minimum friction factor. However, a maximum percentage enhancement of 90.2% is observed due to the presence of miller teeth shaped ribs for e/D=0.042 and P/e=7.14 at Re=3800. With increase in P/e, f tends to decrease due to lesser number of interruptions.

Thermo-Hydraulic Performance Factor

A significant increase in frictional resistance is seen along with the heat transfer augmentation due to the introduction of miller teeth shaped ribs. With the increase in frictional resistance the pumping power increases. So it is necessary to determine the overall performance of a solar air heater.

Table 1 — Variation of performance parameters with different geometrical and operating parameters

Re	e/D=0.021, P/e=14.29			e/D=0.03, P/e=10			e/D=0.042, P/e=7.14			e/D=0.021, P/e=21.43			e/D=0.03, P/e=15			e/D=0.042, P/e=10.7		
	Nu	f	THPF	Nu	f	THPF	Nu	f	THPF	Nu	f	THPF	Nu	f	THPF	Nu	f	THPF
3800	25.4	0.0206	1.233	27.3	0.0249	1.242	30.1	0.0318	1.262	25.4	0.0196	1.249	28.0	0.0235	1.297	30.6	0.0308	1.297
5000	32.4	0.0196	1.282	35.1	0.0246	1.290	38.4	0.0321	1.291	32.1	0.0184	1.300	35.7	0.0229	1.344	38.6	0.0308	1.316
8000	49.8	0.0190	1.358	52.9	0.0248	1.324	55.7	0.0324	1.274	48.8	0.0174	1.371	53.1	0.0226	1.368	55.1	0.0305	1.286
12000	69.8	0.0189	1.359	71.2	0.0245	1.273	71.7	0.0309	1.187	68.2	0.0171	1.375	70.9	0.0222	1.310	70.4	0.0287	1.195
15000	82.0	0.0189	1.325	82.0	0.0239	1.225	81.7	0.0297	1.135	80.3	0.0170	1.344	81.4	0.0217	1.256	80.0	0.0276	1.139
18000	92.8	0.0188	1.289	91.9	0.0234	1.186	90.7	0.0287	1.094	91.0	0.0169	1.309	90.8	0.0213	1.210	88.5	0.0268	1.092
		(a)			(b)			(c)			(d)			(e)			(f)	
Re	e/D=0.021, P/e=28.57			e/D=0.03, P/e=20			e/D=0.042, P/e=14.29			e/D=0.021, P/e=35.7			e/D=0.03, P/e=25			e/D=0.042, P/e=17.86		
	Nu	f	THPF	Nu	f	THPF	Nu	f	THPF	Nu	f	THPF	Nu	f	THPF	Nu	f	THPF
3800	25.1	0.0193	1.245	27.7	0.0229	1.298	30.7	0.0301	1.312	24.9	0.0186	1.249	27.4	0.0215	1.310	30.5	0.0273	1.345
5000	31.6	0.0179	1.292	35.2	0.0220	1.342	38.5	0.0297	1.327	31.2	0.0171	1.292	34.6	0.0204	1.351	38.0	0.0268	1.356
8000	47.4	0.0166	1.356	51.9	0.0214	1.363	54.7	0.0293	1.293	46.3	0.0156	1.350	50.7	0.0196	1.371	54.0	0.0263	1.323
12000	66.2	0.0161	1.362	69.7	0.0210	1.312	69.7	0.0278	1.195	64.4	0.0149	1.358	68.4	0.0191	1.327	68.7	0.0250	1.221
15000	78.3	0.0160	1.338	80.2	0.0207	1.258	78.8	0.0269	1.132	76.3	0.0148	1.339	78.7	0.0188	1.274	77.4	0.0241	1.154
18000	88.9	0.0159	1.305	89.2	0.0203	1.209	87.0	0.0263	1.081	86.9	0.0147	1.311	87.5	0.0184	1.224	85.5	0.0235	1.102
		(g)			(h)			(i)			(j)			(k)			(l)	

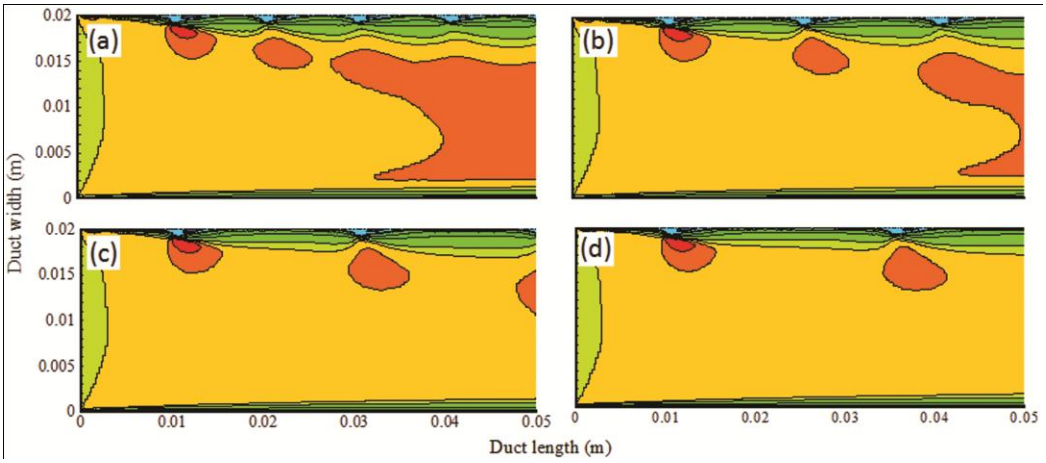

Fig. 3 — Contour of velocity for e/D=0.021 and Re=12000 at different relative pitch ratio (a) P/e= 14.29 (b) P/e= 21.43 (c) P/e= 28.57 (d) P/e= 35.7

$$THPF = \frac{Nu/Nu_s}{(f/f_s)^{1/3}} \quad \ldots (4)$$

Thermo-hydraulic performance factor (THPF) is evaluated by simultaneously considering both thermal and hydraulic performance and is calculated from Eq. (4). In Eq. (4) Nu_s and f_s denotes Nusselt number and friction factor of smooth plate respectively. In the present CFD investigation, it is found that for different geometrical configuration, maximum THPF depends on Re. For e/D=0.021, maximum THPF is noted at Re=12000 for any value of P/e, whereas for e/D=0.03 and 0.042, maximum THPF is observed at Re=8000 and 5000 respectively. A maximum THPF of 1.375 is observed for e/D=0.021 and P/e=21.43 at Re=12000. Table 1 shows the THPF trend for e/D=0.021, 0.03 and 0.042 at different values of P/e and Re.

Conclusions

A 2D CFD simulation of solar air collector with miller teeth shaped ribs is carried out and following key findings can be drawn from the investigation:

- Significant increase in heat transfer characteristics is observed due to vortex formation in the downstream of each rib resulting in enhancement of local turbulent kinetic energy and turbulent kinetic dissipation rate. Reattachment of flow results in breakdown of laminar sub-layer which adds on to the reason for enhancement of heat transfer from the absorber plate. A maximum enhancement of 64.5% in thermal performance is obtained by introducing miller teeth shaped ribs.
- With the introduction of artificial roughness, frictional loss is found to increase due to the increase in flow resistance. A maximum enhancement of 90.2% is noted for e/D value of 0.042 due to higher resisting surface area.
- THPF is analysed to get the optimized geometrical parameter for solar air collector with miller teeth shaped ribs. For same value of e/D and Re, THPF increases with increase in P/e, attains a maximum and then decreases. For e/D=0.021 and P/e=21.43, maximum THPF of 1.375 is observed at Re=12000.

Nomenclature

D	hydraulic diameter, *m*	*Subscript and Greek letters*	
e	eccentricity, *m*	*i*	vector in x-direction
f	friction factor	*j*	vector in y-direction
h	heat transfer coefficient, W/m^2K	*s*	smooth
k	thermal conductivity of air, *W/mK*	*u*	air flow velocity in x-direction, *m/s*
Nu	Nusselt number, (hD/k)	*x,y*	coordinates
P	Pitch, *m*	ρ	air density, kg/m^3
Pr	Prandtl number	μ	dynamic viscosity, Ns/m^2
Re	Reynolds number, (ρuD/μ)	τ	molecular thermal diffusivity
T	Temperature, *K*	τ_t	turbulent thermal diffusivity

References

1 Kumar A, Kumar R, Maithani R, Chauhan R, Kumar S & Nadda R, An experimental study of heat transfer enhancement in an air channel with broken multi type V-baffles, *Heat Mass Transfer*, **53** (2017) 3593-3612.

2 Hans V S, Gill R S & Singh S, Heat transfer and friction factor correlations for a solar air heater duct roughened artificially with broken arc ribs, *Exp Therm Fluid Sci*, **80** (2017) 77-89.
3 Gawande V B, Dhoble A S, Zodpe B B & Chamoli S, Experimental and CFD investigation of convection heat transfer in solar air heater with reverse L-shaped ribs, *Sol Energy*, **131** (2016) 275-295.
4 Yadav A S & Bhagoria J L, A CFD based thermo-hydraulic performance analysis of an artificially roughened solar air heater having equilateral triangular sectioned rib roughness on the absorber plate, *Int J Heat Mass Tran*, **70** (2014) 1016-1039.
5 Chamolia S, Lu R, Xu D & Yu P, Thermal performance improvement of a solar air heater fitted with winglet vortex generators, *Sol Energy*, **159** (2018) 966-983.
6 Kumar R, Goel V, Kumar A, Investigation of heat transfer augmentation and friction factor in triangular duct solar air heater due to forward facing chamfered rectangular ribs: A CFD based analysis, *Renew Energ*, **115** (2018) 824-835.
7 Bezbaruah P, Das R S & Sarkar B K, Thermo-hydraulic performance augmentation of solar air duct using modified forms of conical vortex generators, *Heat Mass Transfer*, **55** (2019) 1387-1403.
8 Lu G & Zhou G, Numerical simulation on performances of plane and curved winglet type vortex generator pairs with punched holes, *Int J Heat Mass Tran*, **102**, (2016) 679-690.
9 Saravanakumar P T & Mayilsami K, Forced convection flat plate solar air heaters with and without thermal storage, *J Sci Ind Res*, **69** (2010) 966-968.
10 Goel A K & Singh S N, Thermal Performance of Solar Air Heater using Jet Impingement Technique with Longitudinal Fins, *J Sci Ind Res*, **76** (2017) 780-784.
11 ASHRAE Standard 93, *Refrig. Air Condition. Eng.* 2003, Atlanta, GA 30329.